Electrochemical behavior of iodide ions in molten fluoride salts

Gabriela Durán-Klie, Davide Rodrigues, Sylvie Delpech

Electrochemical behavior of iodide ions in molten fluoride salts

Gabriela Durán-Klie*, Davide Rodrigues, Sylvie Delpech

Université Paris-Saclay, CNRS/IN2P3, IJCLab, 15 Rue Georges Clémenceau, Orsay 91405, France

Abstract

The electrochemical behavior of iodide ions has been studied in the ternary fluoride salt, LiF-NaF-KF and in the binary salts, LiF-CaF_2 and LiF-ThF_4. The electrochemical study demonstrated that iodide ions are oxidized to produce gaseous species in the three molten fluoride salts. However, the stability of iodide ions was observed to be influenced by the fluroacidity of the molten salt. The efficiency of the extraction of iodide ions was examined in LiF-NaF-KF and LiF-ThF_4. UV-visible spectroscopy was used to quantify the amount of iodide ions oxidized after the execution of several coulometries at applied potential, these coulometries simulated the fluorination step in the reprocessing unit designed for the MSFR. The efficiency of extraction determined in LiF-ThF_4 is higher than 95 % while it is close to 64 % in LiF-NaF-KF at 650°C.

Keywords: iodine, molten fluoride salts, MSFR, fluorination, pyrochemical reprocessing

1. Introduction

The radiological impact of iodine makes of this element one of the more important fission products to take care in the nuclear waste management. As a result of its high chemical reactivity, iodine is present on different forms in the radioactive effluents. For example, in the light-water reactor (LWR), the iodine is stable as molecular iodine (I_2 gas) but it can also be associated to organic molecules (CH_3 gas) and aerosol compounds. Owing to its high mobility and its accumulation capacity (e.g., in the thyroid gland for the human), all transfer mechanisms must be considered for the evaluation of their impact on human healthy and the ecosystems. The ^{129}I is the isotope with the longer period ($t_{1/2}$= $1.57 \cdot 10^7$ years), but other isotopes with a shorter time of live are also produced, as ^{131}I ($t_{1/2}$= 8.02 days), ^{133}I ($t_{1/2}$= 20.8 hours), ^{135}I ($t_{1/2}$= 6.57 hours), ^{132}I ($t_{1/2}$= 2.30 hours) and ^{134}I ($t_{1/2}$= 52.5 minutes) [1]. The isotopes ^{129}I and ^{127}I (stable isotopes) represent 87 % of the total iodine. For example, the potential hazard of the ^{129}I isotope resides in the emission of β and γ radiation of weak energy, making difficult their detection.

Currently, one of the issues associated to the production of nuclear energy is the management of the radioactive waste. For the reactors of fourth generation (GEN IV), the GIF policy group established as a requirement the management and the reduction of long half-life nuclear waste [2, 3]. The Molten Salt Fast Reactor (MSFR) is an innovative concept of GEN IV developed by CNRS since 2004 [4, 5]. Currently, this nuclear concept is studied in the framework of the European project SAMOSAFER of H2020. The MSFR operates with a liquid nuclear fuel consisting of a mixture of fluoride salts LiF-ThF_4-(UF_4/UF_3) (77.5-18.5-4 mol %) melted at high temperature (700-900°C). This reactor is particularly advantageous for the thorium fuel cycle (Th-232/U-233). In addition, the MSFR proposes an integrated reprocessing of the nuclear fuel based on pyrochemical methods to extract the fissile material and to separate the actinides from the fission products. The MSFR satisfies the requirement established for the new generation of nuclear reactors, in terms of durability resource efficiency and decrease of the radiotoxicity of waste.

*Corresponding author.
E-mail address: klie60@gmail.com (G. Durán Klie)

Iodine extraction (^{135}I) was studied by Oak Ridge National laboratory (ORNL) for the Molten Salt Breeder Reactor (MSBR) in LiF-BeF_2 fuel salt [6, 7]. The fast extraction of this isotope should allow decreasing the quantity of ^{135}Xe produced in the nuclear reactor. The methodology developed for the removal of iodine was based in HF sparging. The next equilibrium described the chemical reaction in the fluoride melt:

$$HF\ (g) + I^- \leftrightharpoons F^- + HI\ (g) \quad (1)$$

Another procedure developed by ORNL for the extraction of radionuclides from the fuel consisted in the fluorination. The fluorine production is realized by electrolysis of 2HF-KF molten salt at 368 K. The fluorine gas might to oxide all the elements dissolved in the molten salt until their maximum oxidation state stable in the salt. Several oxidized elements passing into a gaseous state can be separated from the liquid phase. The chemical reactions associated to the fluorination step are:

$$2HF \rightarrow H_2\ (g) + F_2\ (g) \quad (2)$$

$$MF_x + F_2\ (g) \rightarrow MF_{(x+2)}\ (g) \quad (3)$$

In the case of reprocessing scheme developed for the Molten Salt Fast Reactor (MSFR) [5], the fluorination step is also considered for the iodine extraction, as well as some actinides (U, Np and Pu) and other fissions products (Nb, Ru, Te, Mo, Cr, Tc).

The electrochemical behavior of iodine has largely been studied in aqueous media [8–11] but only few studies have been published about its behavior in the molten salts, limiting the research to the molten nitrates [12–14] and chloroaluminates [15, 16]. The studies realized in chloroaluminate melts shown that iodide is oxidized in two steps. The electrochemical process is described by (4) and (5)

$$2I^- \rightarrow I_2 + 2e^- \quad (4)$$

$$I_2 \rightarrow 2I(I) + 2e^- \quad (5)$$

Nevertheless, in molten nitrates, in addition to the oxidation of iodide ions to iodine the formation of triiodide complex has been suggested. To our knowledge, the electrochemical behavior of the iodine has not been studied in the fluorides molten salt.

2. Technical

Materials and Experimental set-up

LiF, NaF, KF, NiF_2, CaF_2 and KI are provided by Sigma Aldrich (> 99.5 % purity). ThF_4 is provided by Solvay-Chemicals. W, Ni, Mo and Au are provided by Goodfellow (> 99.9 % purity). W-Th rod 4 % is provided by CEA (Alternative Energies and Atomic Energy Commission, France). Graphite is provided by Le Carbone-Lorraine (> 98 % purity). HCl 35 % (GPR RECTAPUR) is provided by VWR Chemicals. The storage and handling of all the chemicals are carried out in a glove box in purified argon atmosphere because fluorides have a tendency to absorb water molecules.

Three kinds of molten fluoride salts were studied: LiF-NaF-KF (46.5 – 11.5 – 42) mol % known as FLiNaK, LiF-CaF_2 (79 – 21 mol %) and LiF-ThF_4 (77 – 23 mol %). A same protocol for the preparation of the molten salt mixtures is used. Each mixture is introduced and mixed in a glassy carbon crucible (HTW Hoctemperatur-Werkstoffe GmbH) which is disposed in a cell. The cell is made of quartz and

consists of two parts (top and bottom). The air tightness is maintained using a locking screw. The electrochemical cell is then introduced in a tubular furnace (80cm diameter) connected to a regulation monitor provided by TERMOLAB/Portugal. Electrochemical measurements are performed with a potentiostat-galvanostat model PAR 263A coupled with a PC computer.

The purification of the salt is performed by keeping the cell under vacuum for 24 h at 300 °C. Then, the mixture is melted by increasing the temperature under vacuum. Once the salt is melted, a flow of argon (AlphaGaz1 supplied by Air liquid) is kept throughout the experiment.

The working electrodes are prepared using a W wire (1 mm diameter), a Mo wire (1 mm diameter) and Au wire (1 mm diameter). The gold electrode is chosen as a working electrode because its resistance to the formation of oxide compounds, what allows rising the electroactive domain to anodic potentials. Cathodic potentials are studied with a tungsten or molybdenum electrode. The auxiliary electrode is a graphite rod (3 mm diameter). Three kind of reference electrode were used. They were chosen as a function of the working temperature and their stability in the studied molten fluoride salt. For FLiNaK molten salt, the NiF_2/Ni redox system is chosen as the reference electrode because its reversible charge transfer and good stability in this molten salt [17]. For the electrode preparation, a Pyrex glass tube is filled with FLiNaK molten salt containing 0.01 $mol.kg^{-1}$ of NiF_2 and a Ni wire is dipped inside. A junction potential of 2 mV was measured for this Pyrex glass compartment. For the electrochemical study in LiF-ThF_4 at 650 °C a rod of tungsten-thorium 4% is used as reference electrode. Its stability was verified during 1 week in LiF-ThF_4 at 650 °C. The potential of the cathodic limit given by the reduction of ThF_4 to Th recorded against W-Th reference electrode is -1.567 ± 0.003 V [18]. Finally, Pt wire was used as a pseudo-reference electrode (Pt/PtOx/O^{2-}) in LiF-CaF_2 molten salt. In this work, platinum electrode was chosen because of its high thermal resistance and stability in the molten fluoride salt where the melting point of the eutectic is higher than 600°C (e.g. LiF-CaF_2 [19], LiF-NaF [20]). This electrode was described earlier by Mamantov [21]. A variation of the potential in the order of 10 – 20 mV was recorded in 1 week for the molten LiF-BeF_2-ZrF_4 eutectic. The tightness of the top of the cell is ensuring by introducing electrodes through SVL caps.

Identification of iodide gaseous species generated.

A methodology based on UV-visible spectroscopy measurements was developed to identify the nature of the electrochemical gaseous species produced by the oxidation of I^-. A set of wash bottles containing an aqueous solution of KI were connected to the end of the electrochemical cell to trap the gas produced during the experiments. If iodine gas is produced, the KI aqueous solution (initially colorless) will change to yellow color because the chemical reaction between iodine gas and iodide ions to produce triiodide ions by the following reaction:

$$I^- + I_2\,(g) \leftrightharpoons I_3^- \qquad (6)$$

Triiodide ions presents two spectral bands in the UV-visible region at 288 and 352 nm [22].

Quantification of iodide ions in the molten salt.

A spectrophotometer UV-Visible (Cary 60) provided by Agilent is used for the aqueous analytical measurements of iodide concentration in the molten salt. Quartz SUPRASIL cells provided by HELLMA with 10 mm light path are used. The spectral range is scanned from 500 - 190 nm with a 0.5 nm path length and a slit width of 1 nm. The samples of iodide analyzed are taken by hot sampling in the molten salt. Then the salt is cooled, recovered, and stored under vacuum until its dissolution in HCl aqueous solution. An acid digestion at 80 °C is required for the dissolution of LiF-ThF_4 samples. Then, the measurements are done at room temperature. A solution of KI is used to carry out the

calibration curve realized between 10 and 170 μM. Iodide ions are characterized by UV absorption spectra. The wavelength of maximum absorbance is 226 nm [22].

As described in the relationship 7, the efficiency of extraction of iodine (EEI) is calculated by the ratio between the amount of iodide ions reacted, $n(I^-_{salt})$ (determined by the quantitative analysis of the iodide remained in the molten salt after the electrolysis) and the electric charge measured during the electrolysis, $Q_{electrolysis}$.

$$EEI(\%) = \frac{n(I^-_{salt})}{n(I^-_{consumed})} * 100\%$$

$$= \frac{n(I^-_{salt}) * z * F}{Q_{electrolysis}} * 100\% \quad (7)$$

where, $n(I^-_{consumed})$ is the theoretical amount of iodide consumed during the electrolysis, z is the exchange electron of the electrochemical reaction and F is the Faraday constant.

The overall experimental procedure developed to study the electrochemical behaviour of iodide ions in molten fluoride salt as well as its quantification is summarized in Figure 1.

Thermodynamic diagram of iodide species.
The thermodynamic diagram represents the redox potential against the oxoacidity (E *vs* pa(Li_2O)) of the salt. It is useful to determine the several equilibriums and conditions of stability of iodide species in molten FLiNaK at 650°C.
The steps used for the construction of the thermodynamic diagrams are described in the following:

1. Thermodynamic data for a pure substance is used to calculate the Gibbs free energy and the equilibrium constants for all equilibrium reactions. Thermodynamic data for iodide species was calculated using HSC chemistry 6.0 software [23]
2. The diagram is calculated considering the F_2/F^- as the reference redox system (E = 0V), with an activity for fluoride ions equal to 1 and a pressure of 1 atm for F_2.
3. The activity of soluble species is considered as its molar fraction because the solvation effects are not known in the melt. For the metallic and gaseous species, the activity and the partial pressure are, respectively, 1 and 1 atm.
4. Equilibrium redox potentials, for all equilibrium reactions suggested, were calculated using the Nernst equation (see Table 1).

3. Results and discussion

3.1 Electrochemical behavior of KI in LiF-NaF-KF (46.5-11.5-42 mol %)

Typical cyclic voltammograms recorded on W and Au working electrode in FLiNaK molten salt at 650 °C, with and without KI, are shown in Figure1, in which cathodic (C_x) and anodic (A_x) signals are labeled according to their origin.

The electrochemical behavior of FLiNaK molten salt is shown in Figure 2A. The electroactivity domain is limited to cathodic potentials by the reduction of potassium ions to potassium metal [20]. The redox potential measured for KF/K equilibrium reaction is -1,851 V *vs* NiF_2/Ni. This mechanism of one step is characterized by a reversible charge transfer [24, 25]. The anodic branch of the window potential presents two oxidation signals. The first one (A_2) belongs to the oxidation of oxide ions to oxygen gas

around +0.99 V *vs* NiF_2/Ni. The second signal (A_3) belongs to the oxidation of the gold electrode. So, the anodic limit of the window potential is defined by AuF_2/Au redox system at +1.86 V vs NiF_2/Ni. All electrochemical reactions taking place in FLiNaK at 650°C are written below:

Cathodic potentials

$KF + 1e^- \leftrightharpoons K + F^-$ (7)

Anodic potentials

$2O^{2-} \rightarrow O_2\,(g) + 4e^-$ (8)

$Au + 2F^- \rightarrow AuF_2 + 2e^-$ (9)

The electrochemical behavior of KI in the eutectic FLiNaK molten salt was studied to anodic potentials with the gold working electrode. At the equilibrium potential of the molten salt, iodine is present as iodide ions (I^-). Iodide ions are the more reductive chemical species of iodine. Cyclic voltammogram recorded after the addition of KI (0.044 mol/kg) is shown in Figure 2B. In the forward scan (continuous black line), two new oxidation signals were observed (A_4 and A_5). In the reverse scan (in dotted line on the Figure1B), a third oxidation signal was recorded (A_6). Unlike the electrochemical behavior of iodide ions in chlorides and nitrates molten salt [12–16], the oxidation of iodide ions in FLiNaK is an irreversible electrochemical process characterized by the production of gaseous species.

The identification of the iodine gaseous species was realized by UV-visible analysis after electrolysis at +1.33 V and +1.83 V *vs* NiF_2/Ni. At +1.33 V, a purple gas emission was observed during long times of electrolysis. Purple gas is characteristic of I_2 compound [26]. The formation of I_2 was confirmed by UV-visible spectroscopy measurements from KI aqueous solution, Figure 3. The presence of two absorption bands at 288 and 352 nm confirm the generation of triiodine ions from the chemical reaction (6) between I^- and I_2 produced throughout the electrolysis at low anodic potential. At higher applied potential (+1.83 V) no purple gas production (characteristic of $I_2(g)$) is observed and KI aqueous solution keeps colorless. So, to identify the nature of the compound formed by electrolysis at high applied potential values, the washing bottles were replaced by an aqueous solution of HCl 0.1 M. After the electrolysis, the UV-visible spectrum of HCl solution is modified (Figure 3). The absorption spectrum shows the presence of three new absorption bands (248, 345 and 460 nm). The absorption band at 226 nm is associated to the formation of I^- ions as it can be observed through the spectrum of the control aqueous solution of KI. The absorptions bands observed at 248 nm and 345 nm were associated to the formation of I_2Cl^- and ICl_2^- compound and the absorption band at 460 nm was associated to the formation of I_2 in the acid aqueous solution. The stability of these chloro-complexes of iodide in hydrochloric acid solution was reported earlier by Cason [27]. In the present work, the following chemical reaction is suggested to explain the formation of the chloro-complex of iodide (I_2Cl^-) when gaseous IF species reacts with HCl (10).

$$2IF + 2HCl + Cl^- \rightarrow I_2Cl^- + 2HF + Cl_2(g) \quad (10)$$

The verification of the spontaneity of this reaction was done by the calculation of its free Gibbs energy. The calculated value of ΔG is -94.682 kJ/mol [23]. The chemical equilibrium between I_2Cl^- and I_2 as well as the disproportionation of I_2Cl^- to ICl_2^- and I^- was well explained in Cason's work [27].

The modification of the washing bottle composition demonstrates the formation of a gaseous species containing iodine different from I_2. Based on the thermodynamic diagram of stability of iodine calculated in FLiNaK eutectic at 650°C (Figure 3), we propose an oxidation of iodide to IF(g). The formation of $IF_5(g)$ seems less probable due to the oxidation of gold which occurs at lower potential (dotted line on Figure 3).

The oxidation process of iodide ions in FLiNaK molten salt at 650ºC is described as an oxidation in two steps to produce IF (g). The first step was associated to the oxidation of iodide ions to iodine gas (A_4). The second step corresponds to the oxidation of iodine gas to IF (g) (A_5). Both gaseous species were removed from the gold electrode at the end of the forward scan with the dissolution of the gold working electrode (anodic limit). The renewed gold electrode surface allows the reoxidation of iodide ions during the back scan to produce in one step IF (g) (A_6). Thermodynamic calculations were done to prove the feasibility of the suggested mechanism. The redox potential for the different equilibriums is: -1.607 V for I_2/I^-, -1.348 V for IF/I_2 and -1.443 V for IF/I^-. All potentials are referred to F_2/F^-. Free Gibbs energy for the different chemical equilibriums are reported in Table 1. The electrochemical reactions that take place in FLiNaK are written as:

Forward scan:

$1.1 < E < 1.45$ V/REF $\quad I^- \rightarrow \frac{1}{2}I_2\,(g) + 1e^-$ (11)

$1.5 < E < 2$ V/REF $\quad \frac{1}{2}I_2\,(g) + F^- \rightarrow IF\,(g) + 1e^-$ (12)

Back scan:

1.62 V/REF $\quad I^- + F^- \rightarrow IF\,(g) + 2e^-$ (13)

The extraction efficiency of iodine calculated considering the charge imposed to the system during the electrolysis and the I^- ions not consumed by electrolysis at different potentials is presented in Table 2. For the electrolysis performed with an applied voltage lower than 1.45 V/REF, the number of exchanged electrons used was one (as show in the reaction 11). On the other hand, n=2 was used for the electrolysis performed with an anodic potential higher than 1.5V/REF. as observed in the global electrochemical reaction:

$$I^- + F^- \rightarrow IF\,(g) + 2e^- \quad (14)$$

The efficiency of the process depends on the potential applied. At higher anodic potentials applied, the efficiency is above 60%.

3.2 Electrochemical behavior of KI in LiF-CaF_2 (79 – 21 mol %) at 830ºC.

A typical cyclic voltammogram recorded in the eutectic LiF-CaF_2 molten salt is shown in Figure 5A. An electroactivity domain of 4.21 V was determined. Cathodic and anodic limits belong to the reduction of lithium ions to lithium metal at -1.68 V *vs* Pt, and the oxidation of the gold working electrode at +2.53 V *vs* Pt [28]. The oxidation of oxide ions to oxygen gas was characterized by the presence of an anodic pic at +1.6V *vs* Pt.

Cyclic voltammograms recorded in the binary LiF-CaF_2 in the presence of KI are shown in Figure 5B. The oxidation of iodide ions to iodine (A4) was observed at anodic potentials higher than 1 V vs Pt. The oxidation of iodide ions in this melt is described as an irreversible system taking place in one step. The fluctuation of the density current is associated to the gas evolution. Unlike the chemical behavior observed in FLiNaK molten salt, iodide ions are not stable in LiF-CaF_2. A decrease with time of the density of current of the oxidation signal A_4 was observed, accompanied by the evolution of a purple gas. The spontaneous oxidation of iodide ions has been associated to the presence of oxygen (O_2) traces in the media, which is introduced with the argon atmosphere. Unlike molten FLiNaK, the redox couple $O_2(g)/O^{2-}$ is more oxidant than $I_2(g)/I^-$. This inversion of the redox potential leads to the chemical oxidation of iodide ions when oxygen is present in the cover atmosphere. The increase of

the redox potential $O_2(g)/O^{2-}$ can be due to the increase of the stability of oxide ions in LiF-CaF_2 compared to FLiNaK. This behavior is explained by the difference on the fluoroacidity of both melts. The fluoroacidity notion in molten fluoride salts is related with the amount of free fluoride ions in the melt which define its activity ($a(F^-)$) in the molten salt. Several works demonstrated that the fluoroacidity of the molten salt depends of their composition (type of cations and molar ratio). FLiNaK molten salt is considered as a fluorobasic salt. In this case, all cations are dissociated and the amount of free fluoride ions is very high, making its activity close to 1. In the case of LiF-CaF_2, a high fluoroacidity was reported by Kergoat [29, 30]. A fluoroacidic molten salt promotes the formation of fluoro-complex species making the activity of fluoride ions lower than 1. Therefore, in LiF-CaF_2, the oxide ions are higher solvated than in a basic salt such as FLiNaK.

A preliminary kinetic study was realized to demonstrate the influence of oxygen gas on the oxidation of iodide ions added to LiF-CaF_2 molten salt. Two qualities of Ar gas have been used in this study: Ar-AlphaGaz1 (O_2 <2ppm) and Ar-AlphaGaz2 (O_2 <0.1 ppm). The amount of iodide in the salt has been deduced from the quantitative analysis of of triiodide ions produced in the wash bottles. The reaction rate relationship for the chemical reaction expressed by the equilibrium (6) shows that the kinetic oxidation of iodide ions in LiF-CaF_2 follows a pseudo first order reaction rate with respect to iodide ions (17).

$$\boldsymbol{v = k * [I^-] * [I_2]} \quad (15)$$

$$\boldsymbol{k' = k * [I_2]} \quad (16)$$

$$\boldsymbol{v = k' * [I^-]} \quad (17)$$

Experimental results showed in Figure 6 were fitted with a first order reaction using the following lineal kinetic expression (18)

$$\boldsymbol{ln(n\, I^-) = ln(n\, I^-)_0 - k't} \quad (18)$$

Where, $(n\ I^-)_o$ is the initial amount of iodide ions in melt (mol), (I^-) is the amount of iodide ions at time *t* (mol), *t* is the time (s) and *k'* is the pseudo kinetic constant (s^{-1}).
Kinetic results for the oxidation of I^- in LiF-CaF_2 molten salt are summarized in Table 3.

3.3 Electrochemical behavior of KI in LiF-ThF_4 (77-23 mol %) at 650°C.

Typical cyclic voltammograms recorded in LiF-ThF_4 molten salt without KI on Mo and Au working electrodes are given in Figure 7A. The electroactivity domain is limited at cathodic potentials by the reduction of thorium ions to thorium metal (C_1). The electrodeposition of thorium metal was confirmed by XRD [31]. The electrochemical response of ThF_4/Th redox system (-1.59 V *vs* W/Th) is characteristic of a reversible charge transfer in one step. In the same way as the electrochemical response obtained in FLiNaK and LiF-CaF_2 molten salt, the anodic branch is limited by the oxidation of the gold electrode (A_3) at 2.25 V *vs* W/Th. The oxidation signal (A_2) observed at 1.25 V *vs* W/Th belongs to the oxidation of oxide ions to oxygen gas. Comparing the electrochemical response of oxide free ions in FLiNaK and LiF-ThF_4 molten salt, an anodic shift of the potential of the couple O_2/O^{2-} was observed. The shift of 59 mV[1] is associated to a higher cationic solvation of oxide ions in LiF-ThF_4 compare with the ternary salt. Thermodynamic calculations show that in a molten salt

[1] The potential measured against W/Th are referred to NiF_2/Ni reference electrode to compare the results obtained in FLiNaK and LiF-ThF_4 molten salts.

containing oxides the formation of a thorium oxyfluoride compound ($ThOF_2$) is expected [23]. As in molten LiF-CaF_2 eutectic, the fluoroacidity of the salt plays an important role in the stabilization of oxide ions in the melt. In an acid fluoride molten salt as LiF-ThF_4, the first chemical specie oxidized is the oxyfluoride compound instead the free oxide ions.

A new oxidation signal (A4) is observed after addition of KI in the binary LiF-ThF_4 molten salt, (Figure 7B). The oxidation of iodide ions involves a mechanism in one-step to produce iodine gas at anodic potential higher than +0,53V vs W/Th. In the same way to the behavior observed in LiF-CaF_2 melt, iodine gas is also generated by the chemical oxidation of iodide ions in presence of oxygen traces in the cover gas. A continuous decrease of the oxidation current density of iodide ions was observed throughout the study. Through the analysis of the cyclic voltammogram, it is evident than the electrochemical and chemical behavior of the iodide ions is similar in both fluoroacid molten LiF-ThF_4 and LiF-CaF_2. This conclusion can be supported by the recent work published by Souček [32]. It was demonstrated that the amount of free fluorine ions was comparable in both salts. They found a similar activity coefficient for ThF_4 dissolved in LiF-CaF_2 and LiF-ThF_4 showing the similar affinity of this cation for free fluoride ions. A different activity coefficient of ThF_4 was reported previously in FLiNaK [31].

Reaction mechanisms were elucidated by electrolysis on a gold electrode at +1.05 and +1.85 V *vs* W/Th. The evolution of the electric charge consumed during the electrolysis against the quantity of iodide ions oxidized is presented Figure 8. The number of electrons exchanged by mole of iodide ion oxidized determined for all the redox potentials applied is equal to 1, indicating the formation of iodine gas in all the potential window considered.

Throughout the electrolysis at +1.85 V vs W/Th, two electrochemical reactions can take place: (i) the oxidation of iodide ions to iodine gas, and (ii) the oxidation of oxide ions to oxygen. At the same time, the oxygen generated during the electrolysis react with the iodide ions presents into the melt. Consequently, the reactions associated to the second oxidation signal (A_2) are:

$$I^- \rightarrow \tfrac{1}{2} I_2\,(g) + 1e^- \qquad (19)$$

$$ThOF_2 + 2F^- \rightarrow \tfrac{1}{2} O_2\,(g) + ThF_4 + 2e^- \qquad (20)$$

$$\tfrac{1}{2} O_2\,(g) + ThF_4 + 2I^- \rightarrow I_2\,(g) + ThOF_2 + 2F^- \qquad (21)$$

And the global reaction is:

$$3I^- \rightarrow {}^{3}/_{2} I_2\,(g) + 3e^- \qquad (22)$$

A global extraction efficiency of iodide ions was calculated for both electrolysis conditions in LiF-ThF_4 at 650°C (Table 4). A higher efficiency of extraction was determined at high anodic potentials.

The kinetic of the oxidation of the iodide was studied using an atmosphere of argon gas with an oxygen content lower than 2ppm and an atmosphere of hydrogenated argon (95%Ar, 5%H_2) with an oxygen content up to 5 ppm. The chemical reaction (24) was used to stablish the reaction rate relationship (26)

$$\boldsymbol{v = k * [I^-]^2 * P(O_2)^{1/2} * [ThF_4]} \qquad (23)$$

$$\boldsymbol{k' = k * P(O_2)^{1/2} * [ThF_4]} \quad (24)$$

$$\boldsymbol{v = k' * [I^-]^2} \quad (25)$$

where the partial pressure of oxygen and the concentration of ThF_4 are constants. Then the reaction rate can be rewritten as a function of a pseudo second order rate constant (k') with respect to iodide ions. Finally, the reaction rate can be expressed by equation (28)

For both experimental conditions, a kinetic of secondary order was used to simulate the oxidation of the iodide ions in LiF-ThF_4, Figure 9. The lineal kinetic relation is written as:

$$\boldsymbol{\frac{1}{[I^-]} = \frac{1}{[I^-]_o} + k't} \quad (26)$$

Where, $[I^-]_o$ is the initial concentration of iodide ions in melt (mol/cm^3), $[I^-]$ is the concentration of iodide ions at time *t* (mol/cm^3), *t* is the time (s) and *k'* is the pseudo kinetic constant (cm^3/mol^1.s^1).

A slower kinetic reaction is observed when the system was in contact with the hydrogenated argon, suggesting a higher stability of iodine ions in the melt. The decrease of the kinetic of oxidation of iodine ions is associated to the partial decrease of iodine gas by recombination with the hydrogenated cover atmosphere ($H_2 + I_2 \rightarrow 2HI$). The half-live of the reaction as well as the kinetic constants are summarized in Table 5.

4. Conclusion

The electrochemical behavior of iodide was studied in three different molten fluoride salts, FLiNaK, LiF-CaF_2 and LiF-ThF_4. A remarkable difference of the electrochemical behavior and stability of iodide ions was found depending on the fluoride salts studied. The chemistry of iodide ions is much simpler in the molten medias with a higher fluoroacidity. In a fluorobasic molten salt such as (FLiNaK), iodide ions are stable and can be oxidized to IF (g) in a mechanism of two steps. However, in the fluoroacidic molten salts such as LiF-CaF_2 and LiF-ThF_4, iodide ions can be spontaneously oxidized to iodine gas in the presence of oxygen. The chemical oxidation of the iodide ions can be explained by the high stability of oxyfluoride ions in the fluoroacidic molten medias leading to increase the oxidation power of O_2(g). Oxyfluoride ions are more stable than the oxide free ions present in FLiNaK producing an inversion of the redox potential of O_2/O^{2-} and I_2/I^- redox couple (Figure 10). In LiF-CaF_2, the solvation of oxide ions is higher leading to an increase of the potential of O_2(g)/O^{2-} redox system. Under this condition, the presence of oxygen traces will produce the oxidation of the more reducing species.

The electrolysis executed in LiF-ThF_4 showed that almost all iodide ions can be extracted as iodine gas. The extraction of iodide ions by electrochemistry allow to validate the extraction of this species by a fluorination step on the reprocessing system of the MSFR.

References

1. Hu, Q., & Moran, J. E. (2010). Iodine: Radionuclides. In *Encyclopedia of Inorganic Chemistry*. John Wiley & Sons, Ltd. https://doi.org/10.1002/0470862106.ia724

2. Serp, J., Allibert, M., Beneš, O., Delpech, S., Feynberg, O., Ghetta, V., … Zhimin, D. (2014). The molten salt reactor (MSR) in generation IV: Overview and perspectives. *Progress in Nuclear Energy*, *77*, 308–319. https://doi.org/10.1016/j.pnucene.2014.02.014
3. Boussier, H., Delpech, S., Ghetta, V., Heuer, D., Holcomb, D. E., Ignatiev, V., … Serp, J. (2012). The Molten Salt Reactor (MSR) in Generation IV: Overview and Perspectives (pp. 1–15). Presented at the GIF Symposium - San Diego (California), San Diego (California).
4. Merle-Lucotte, E., Heuer, D., Brovchenko, M., & Ghetta, V. (2011). Launching the thorium fuel cycle with the Molten Salt Fast Reactor. In *Proceedings of ICAPP 2011*. Nice, France.
5. Delpech, S., Merle-Lucotte, E., Heuer, D., Allibert, M., Ghetta, V., Le-Brun, C., … Picard, G. (2009). Reactor physic and reprocessing scheme for innovative molten salt reactor system. *Journal of Fluorine Chemistry*, *130*(1), 11–17. https://doi.org/10.1016/j.jfluchem.2008.07.009
6. Briggs, R. B. (1965). *Molten Salt Reactor Program Semiannual Progress Report (ORNL-3872)*.
7. Grimes, W. R. (1966). *Molten-Salt Reactor Program Semiannual Progress Report (ORNL-4076)*.
8. Dané, L. M., Janssen, L. J. J., & Hoogland, J. G. (1968). The iodine/iodide redox couple at a platinum electrode. *Electrochimica Acta*, *13*(3), 507–518. https://doi.org/10.1016/0013-4686(68)87022-7
9. Grgur, B. N., Gvozdenović, M. M., Stevanović, J. S., Jugović, B. Z., & Trišović, Lj. T. (2006). Electrochemical oxidation of iodide in aqueous solution. *Chemical Engineering Journal*, *124*(1), 47–54. https://doi.org/10.1016/j.cej.2006.08.028
10. Janssen, L. J. J., & Blijlevens, M. H. A. (2003). Electrochemical oxidation of iodate to periodate. *Electrochimica Acta*, *48*(25), 3959–3964. https://doi.org/10.1016/S0013-4686(03)00535-8
11. Shu, Z. X., & Bruckenstein, S. (1991). Iodine adsorption studies at platinum. *Journal of Electroanalytical Chemistry and Interfacial Electrochemistry*, *317*(1), 263–277. https://doi.org/10.1016/0022-0728(91)85019-L
12. Sacchetto, G. A., Bombi, G. G., & Fiorani, M. (1969). Standard electrode potentials of the iodine-iodide system in molten (Li,K)NO3. *Journal of Electroanalytical Chemistry and Interfacial Electrochemistry*, *20*(1), 89–98. https://doi.org/10.1016/S0022-0728(69)80010-0

13. Swofford, H. S., & Propp, J. H. (1965). A Voltammetric Study of the Oxidation of Iodide and Bromide in Potassium Nitrate-Sodium Nitrate Eutectic Melts. *Analytical Chemistry*, *37*(8), 974–977. https://doi.org/10.1021/ac60227a006
14. Triaca, W. E., Videla, H. A., & Arvía, A. J. (1971). Electrochemical oxidation of iodide dissolved in sodium-nitrate-potassium-nitrate eutectic melt on a platinum rotating disk electrode. *Electrochimica Acta*, *16*(10), 1671–1682. https://doi.org/10.1016/0013-4686(71)85078-8
15. Marassi, R., Mamantov, G., & Chambers, J. Q. (1975). Electrochemical behavior of iodine, sulfur and selenium in AlCl3□NaCl melts. *Inorganic and Nuclear Chemistry Letters*, *11*(4), 245–252. https://doi.org/10.1016/0020-1650(75)80085-7
16. Marassi, R., Chambers, J. Q., & Mamantov, G. (1976). Electrochemistry of iodine and iodide in chloroaluminate melts. *Journal of Electroanalytical Chemistry and Interfacial Electrochemistry*, *69*(3), 345–359. https://doi.org/10.1016/S0022-0728(76)80135-0
17. Jenkins, H. W., Mamantov, G., & Manning, D. L. (1968). E.M.F. measurements on the nickel-nickel(II) couple in molten fluorides. *Journal of Electroanalytical Chemistry and Interfacial Electrochemistry*, *19*(4), 385–389. https://doi.org/10.1016/S0022-0728(68)80101-9
18. Durán-Klie, G. (2017). *Étude du comportement de l'uranium et de l'iode dans le mélange de fluorures fondus LiF-ThF_4 à 650 °C. Université Paris-Saclay.* Université Paris-Saclay, 2017.
19. Gibilaro, M., Massot, L., & Chamelot, P. (2015). A way to limit the corrosion in the Molten Salt Reactor concept: the salt redox potential control. *Electrochimica Acta*, *160*, 209–213. https://doi.org/10.1016/j.electacta.2015.01.142
20. Massot, L., Cassayre, L., Chamelot, P., & Taxil, P. (2007). On the use of electrochemical techniques to monitor free oxide content in molten fluoride media. *Journal of Electroanalytical Chemistry*, *606*(1), 17–23. https://doi.org/10.1016/j.jelechem.2007.04.005
21. Mamantov, Gleb., & Manning, D. L. (1966). Voltammetry and Related Studies of Uranium in Molten Lithium Fluoride-Beryllium Fluoride-Zirconium Fluoride. *Analytical Chemistry*, *38*(11), 1494–1498. https://doi.org/10.1021/ac60243a010

22. Kireev, S. V., & Shnyrev, S. L. (2015). Study of molecular iodine, iodate ions, iodide ions, and triiodide ions solutions absorption in the UV and visible light spectral bands. *Laser Physics*, *25*(7), 075602. https://doi.org/10.1088/1054-660X/25/7/075602
23. Roine, A. (2006). HSC Chemistry 6.0". Outokumpu Research OY, Pori, Finland. Finland.
24. Qiao, H., Nohira, T., & Ito, Y. (2003). Electrochemical Behavior of Oxide Ion at a Glassy Carbon Electrode in a LiF-NaF-KF Eutectic Melt. *Electrochemistry*, *71*(7), 530–535. https://doi.org/10.5796/electrochemistry.71.530
25. Durán-Klie, G., Rodrigues, D., & Delpech, S. (2016). Dynamic Reference Electrode development for redox potential measurements in fluoride molten salt at high temperature. *Electrochimica Acta*, *195*, 19–26. https://doi.org/10.1016/j.electacta.2016.02.042
26. Rolsten, R. F. (1961). *Iodide metals and metal iodides*. New York, NY: Wiley.
27. Cason, D. L., & Neumann, H. M. (1961). Stability of the Chloro-complexes of Iodine in Aqueous Solution1. *Journal of the American Chemical Society*, *83*(8), 1822–1828. https://doi.org/10.1021/ja01469a013
28. Massot, L., Chamelot, P., Gibilaro, M., Cassayre, L., & Taxil, P. (2011). Nitrogen evolution as anodic reaction in molten LiF–CaF2. *Electrochimica Acta*, *56*(14), 4949–4952. https://doi.org/10.1016/j.electacta.2011.03.131
29. Kergoat, M., Gibilaro, M., Massot, L., & Chamelot, P. (2015). Generalized method for determining fluoroacidity by electrochemical diffusion coefficient measurement (application to HfF4). *Electrochimica Acta*, *176*, 265–269. https://doi.org/10.1016/j.electacta.2015.06.124
30. Kergoat, M., Massot, L., Gibilaro, M., & Chamelot, P. (2014). Investigation on fluoroacidity of molten fluorides solutions in relation with mass transport. *Electrochimica Acta*, *120*, 258–263. https://doi.org/10.1016/j.electacta.2013.12.035
31. Rodrigues, D. (2015, December 4). *Solvatation du thorium par les fluorures en milieu sel fondu à haute température : application au procédé d'extraction réductrice pour le concept MSFR* (phdthesis). Université Paris Sud-Université Paris Saclay. Retrieved from https://tel.archives-ouvertes.fr/tel-01250763/document

32. Souček, P., Rodrigues, D., Beneš, O., Delpech, S., Rodrigues, A., & Konings, R. J. M. (2021). Electrochemical measurements of LiF-CaF2-ThF4 melt and activity coefficient of ThF4 in LiF-CaF2 eutectic melt. *Electrochimica Acta*, *380*, 138198. https://doi.org/10.1016/j.electacta.2021.138198

Figures and Tables:

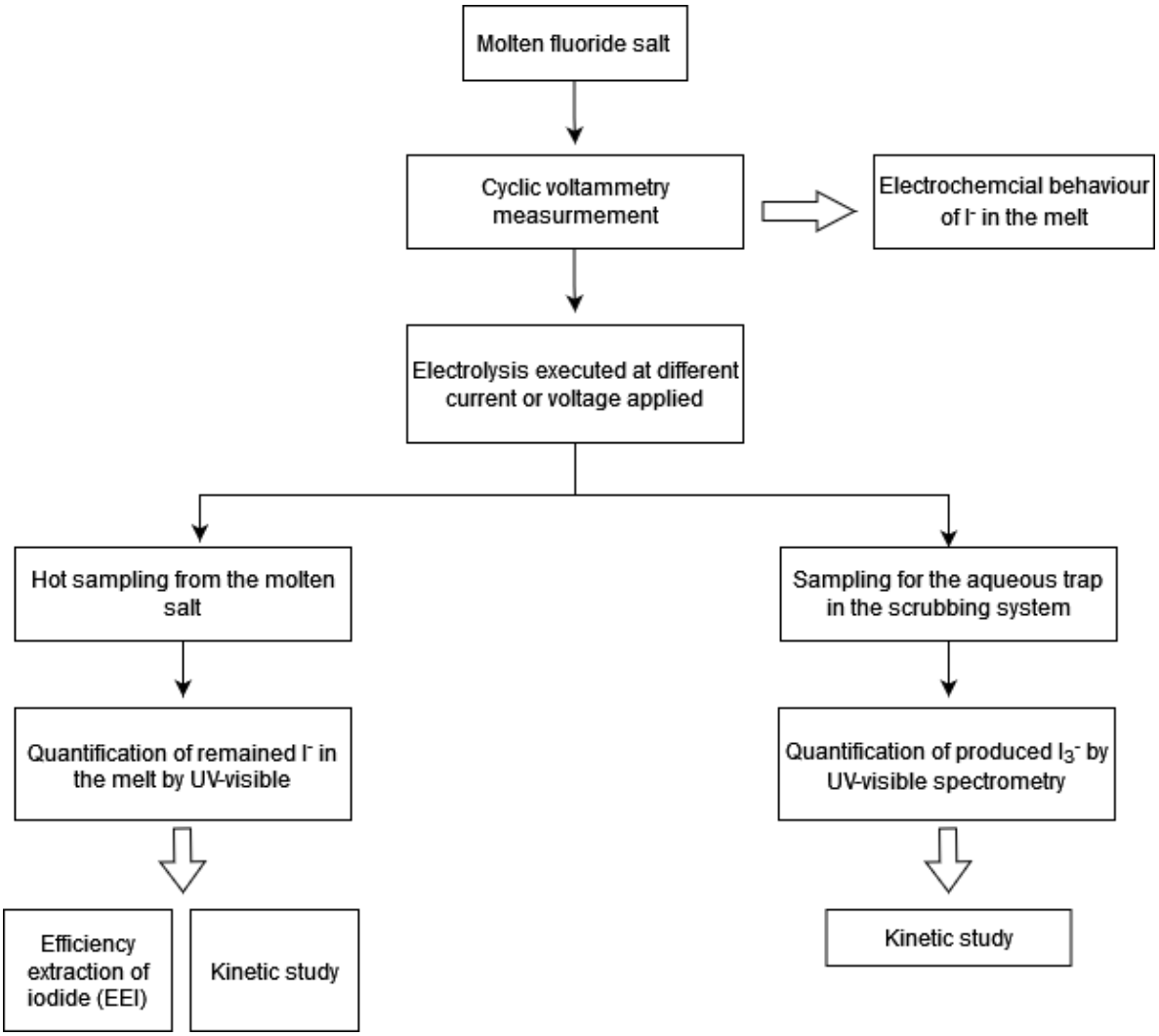

Figure 1. Schematic diagram representing the experimental procedure followed for the study and quantification of iodide ions in the molten fluoride melts.

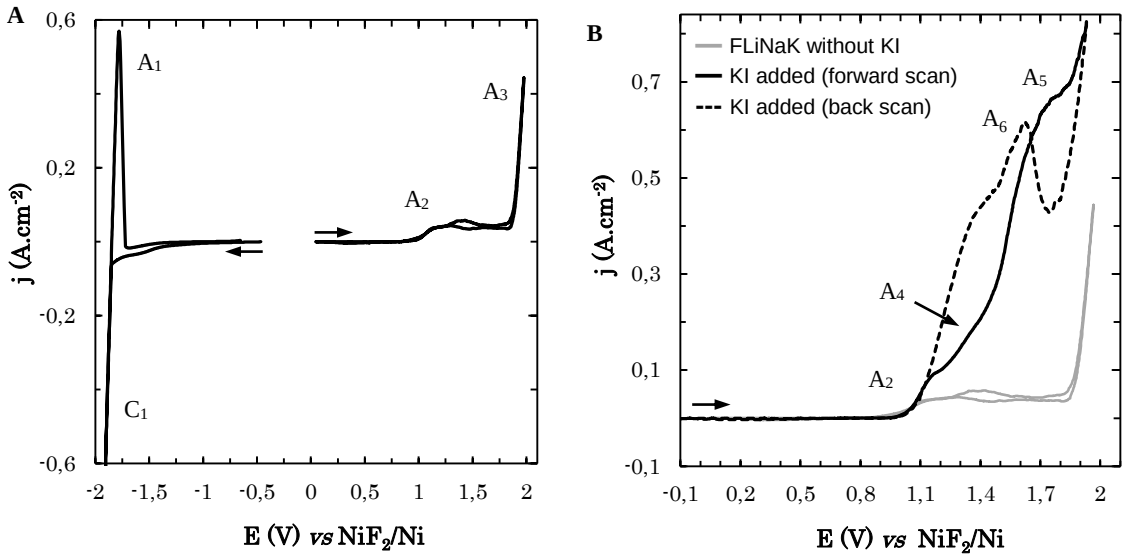

Figure 2. Cyclic voltammograms recorded at 100 mV/s in LiF-NaF-KF (46.5-11.5-42 mol %) at 650°C without (A) and with KI (0.044 mol/kg) (B) at 650°C on a tungsten electrode (cathodic potentials) and on a gold electrode (anodic potentials). S_{el} = 0.33 cm^2

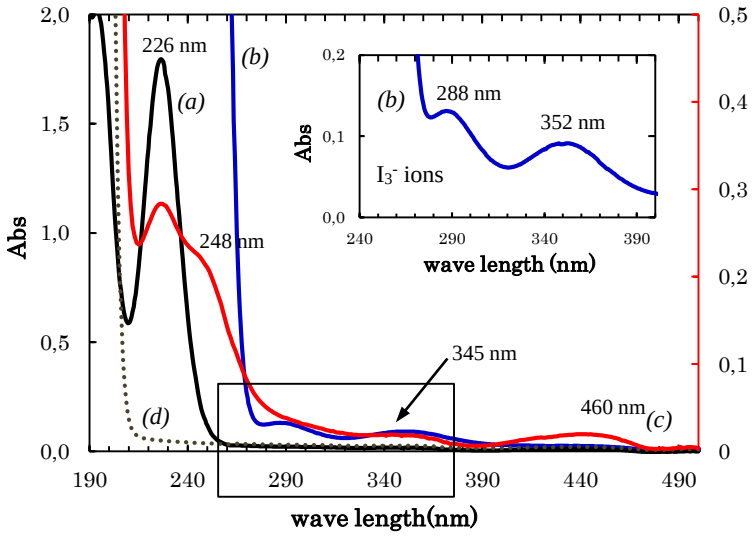

Figure 3. UV-visible spectra of several aqueous solutions containing iodine ions: *(a)* KI aqueous solution (89 μM), *(b)* KI aqueous solution in contact with iodine gaseous species generated at +1.3V, *(c)* HCl aqueous solution (0.1 M) in contact with iodine gaseous species generated at +1.83 V, *(d)* Dash line corresponding to HCl aqueous solution (0.1 M).

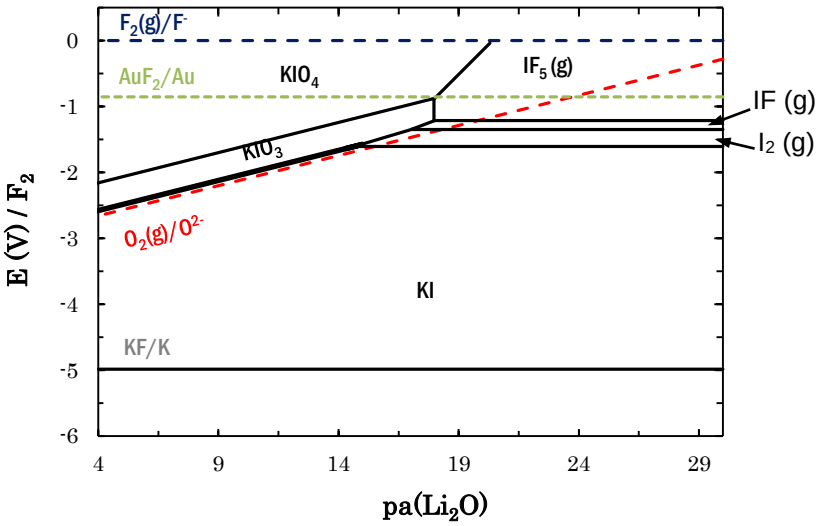

Figure 4. Thermodynamic diagram (E *vs* pa(Li_2O)) of iodide species in molten LiF-NaF-KF eutectic calculated at 650°C. The concentration of soluble iodide species in the equilibrium condition was fixed at 0.16 mol%.

Table 1. Nernst relations and chemical equilibriums of several chemical species considered for the construction of the thermodynamic diagram in LiF-NaF-KF eutectic at 650°C. The constant m in the Nernst relation is equal to 2.3RT/F.

Electrochemical system and chemical reaction	Nernst relation and chemical equilibrium	ΔG (kJ/mol) or log K
$\frac{1}{2}I_2$ (g) + 1e$^-$ → I$^-$ $\frac{1}{2}I_2$ (g) + KF → KI + $\frac{1}{2}F_2$ (g)	$E_1 = E^\circ_{\left(\frac{I_2}{I^-}\right)} + m log \frac{P(I_2)^{\frac{1}{2}}}{a(I^-)}$	197.681
IF (g) + 1e$^-$ → $\frac{1}{2}I_2$ (g) + F$^-$ IF (g) → $\frac{1}{2}I_2$ (g) + $\frac{1}{2}F_2$ (g)	$E_2 = E^\circ_{\left(\frac{IF}{I_2}\right)} + m log \frac{P(IF)}{P(I_2)^{\frac{1}{2}} * a(F^-)}$	130.092
IF_5 (g) + 4e$^-$ → IF (g) + 4F$^-$ IF_5 (g) → IF (g) + $2F_2$ (g)	$E_3 = E^\circ_{\left(\frac{IF_5}{IF}\right)} + \frac{m}{4} log \frac{P(IF_5)}{P(IF) * a(F^-)^4}$	467.484
IO_3^- + 6LiF + 6e$^-$ → I$^-$ + $3Li_2O$ + 6F$^-$ KIO_3 + 6LiF → KI + $3Li_2O$ + $3F_2$ (g)	$E_4 = E^\circ_{\left(\frac{IO_3^-}{I^-}\right)} + \frac{m}{6} log \frac{a(IO_3^-) * a(LiF)^6}{a(I^-) * a(Li_2O)^3 * a(F^-)^6}$	1669.977
IO_3^- + 6LiF + 5e$^-$ → $\frac{1}{2}I_2$ (g) + $3Li_2O$ + 6F$^-$ KIO_3 + 6LiF → $\frac{1}{2}I_2$ (g) + $3Li_2O$ + KF + 5/$2F_2$ (g)	$E_5 = E^\circ_{\left(\frac{IO_3^-}{I_2}\right)} + \frac{m}{5} log \frac{a(IO_3^-) * a(LiF)^6}{P(I_2)^{\frac{1}{2}} * a(Li_2O)^3 * a(F^-)^6}$	1472.296
IO_3^- + 6LiF + 4e$^-$ → IF (g) + $3Li_2O$ + 5F$^-$ KIO_3 + 5LiF → IF (g) + $3Li_2O$ + KF + $2F_2$ (g)	$E_6 = E^\circ_{\left(\frac{IO_3^-}{IF}\right)} + \frac{m}{4} log \frac{a(IO_3^-) * a(LiF)^6}{P(IF) * a(Li_2O)^3 * a(F^-)^5}$	1342.205
KIO_3 + 6LiF → IF_5 (g) + $3Li_2O$ + KF	$K_7 = \frac{P(IF_5) * a(Li_2O)^3 * a(KF)}{a(KIO_3) * a(LiF)^6}$	-49.499
IO_4^- + 2LiF + 2e$^-$ → IO_3^- + Li_2O + 2F$^-$ KIO_4 + 2LiF → KIO_3 + Li_2O + F_2 (g)	$E_8 = E^\circ_{\left(\frac{IO_4^-}{IO_3^-}\right)} + \frac{m}{2} log \frac{a(IO_4^-) * a(LiF)^2}{a(IO_3^-) * a(Li_2O) * a(F^-)^2}$	474.903
IO_4^- + 8LiF + 2e$^-$ → IF_5 (g) + $4Li_2O$ + 3F$^-$ KIO_4 + 8LiF → IF_5 (g) + $4Li_2O$ + KF + F_2 (g)	$E_9 = E^\circ_{\left(\frac{IO_4^-}{IF_5}\right)} + \frac{m}{2} log \frac{a(IO_4^-) * a(LiF)^8}{P(IF_5) * a(Li_2O)^4 * a(F^-)^3}$	1349.624
KF + 1e$^-$ → K + F$^-$ KF → K + $\frac{1}{2}F_2$ (g)	$E_{10} = E^\circ_{\left(\frac{KF}{K}\right)} + m log \frac{a(KF)}{a(K) * a(F^-)}$	474.405
$\frac{1}{2}O_2$ (g) + 2LiF + 2e$^-$ → Li_2O + 2F$^-$ $\frac{1}{2}O_2$ (g) + 2LiF → Li_2O + F_2 (g)	$E_{11} = E^\circ_{\left(\frac{O_2}{Li_2O}\right)} + \frac{m}{2} log \frac{a(LiF)^2 * P(O_2)^{\frac{1}{2}}}{a(Li_2O) * a(F^-)^2}$	579.301
IF (g) + 2e$^-$ → I$^-$ + F$^-$ IF (g) + KF→ KI + F_2 (g)	$E_{12} = E^\circ_{\left(\frac{IF}{I^-}\right)} + \frac{m}{2} log \frac{P(IF)}{a(I^-) ** a(F^-)}$	327.772

Table 2. Iodine extraction efficiency by electrolysis at different applied potentials in FLiNaK molten salt at 650°C for 20 minutes.

E (V) vs NiF_2/Ni	Iodine extraction (%)
1.33	40 ± 5
1.73 – 1.83	64 ± 5

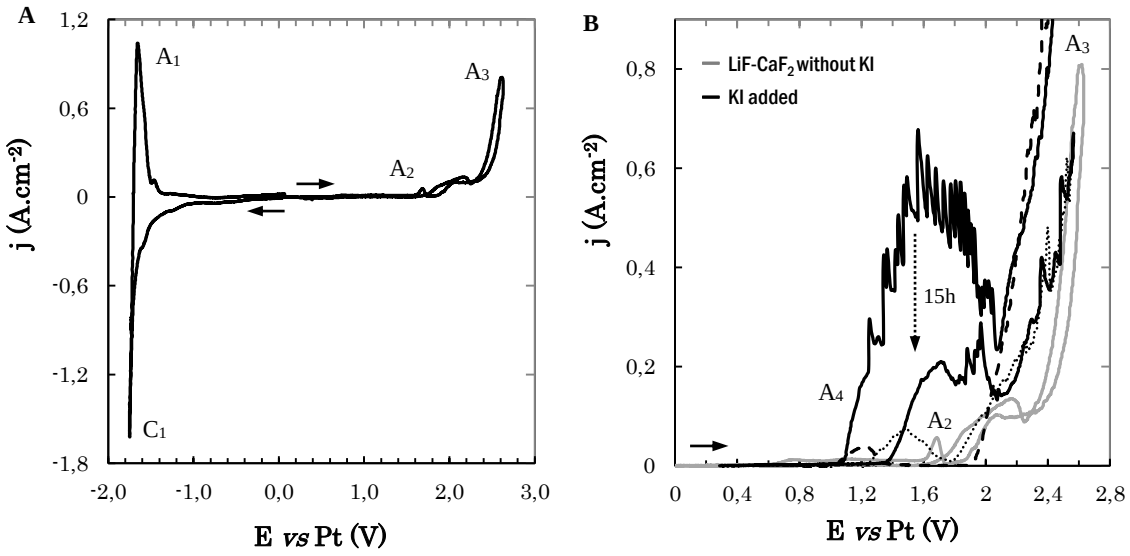

Figure 5. Cyclic voltammograms recorded at 100 mV/s in LiF-CaF_2 (79 - 21 mol %) on a tungsten electrode (S=0.17 cm^2) (cathodic part) and on a gold electrode (S=0.23 cm^2) (anodic part) (A) without and (B) with KI (0.016mol/kg) at 830°C under. Discontinuous line shows the reverse scan. 15 hours after the first addition of KI in LiF-CaF_2 a decrease of the density of current of the CV was recorded on the gold working electrode.

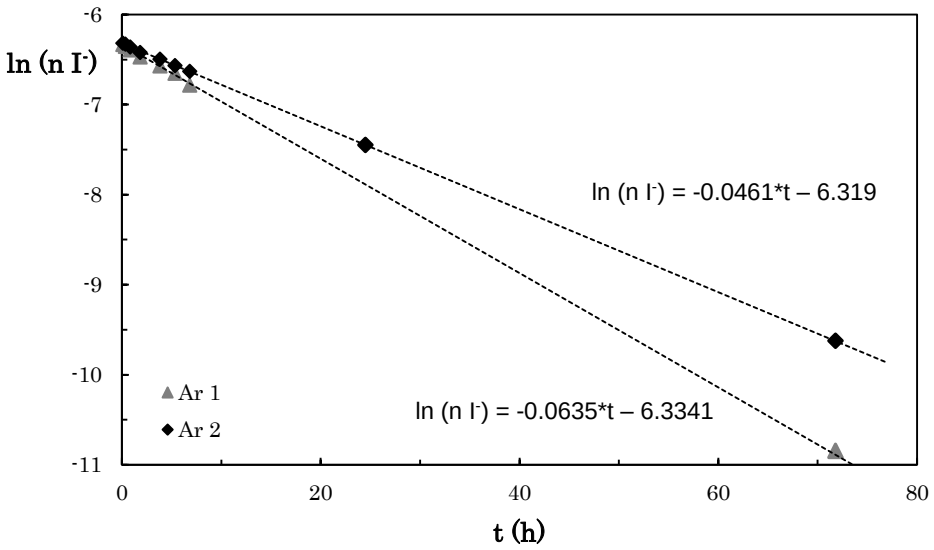

Figure 6. Temporal evolution of the quantity of iodide ions (mole) in LiF-CaF_2 molten salt at 830°C under an argon atmosphere containing two different amounts of oxygen. Argon Alphagaz1: O_2 < 2 ppm and Argon Alphagaz2: O_2 < 0.1 ppm.

Table 3. Oxidation kinetic constants of iodide ions and half-life in LiF-CaF_2 at 830°C, under an argon atmosphere containing two different amounts of oxygen.

Oxygen content	k (s^{-1})	$t_{1/2}$ (h)
Argon 1 / O_2 < 2 ppm	$1.76.10^{-5}$	10.92
Argon 2 / O_2 < 0.1 ppm	$1.28.10^{-5}$	15.04

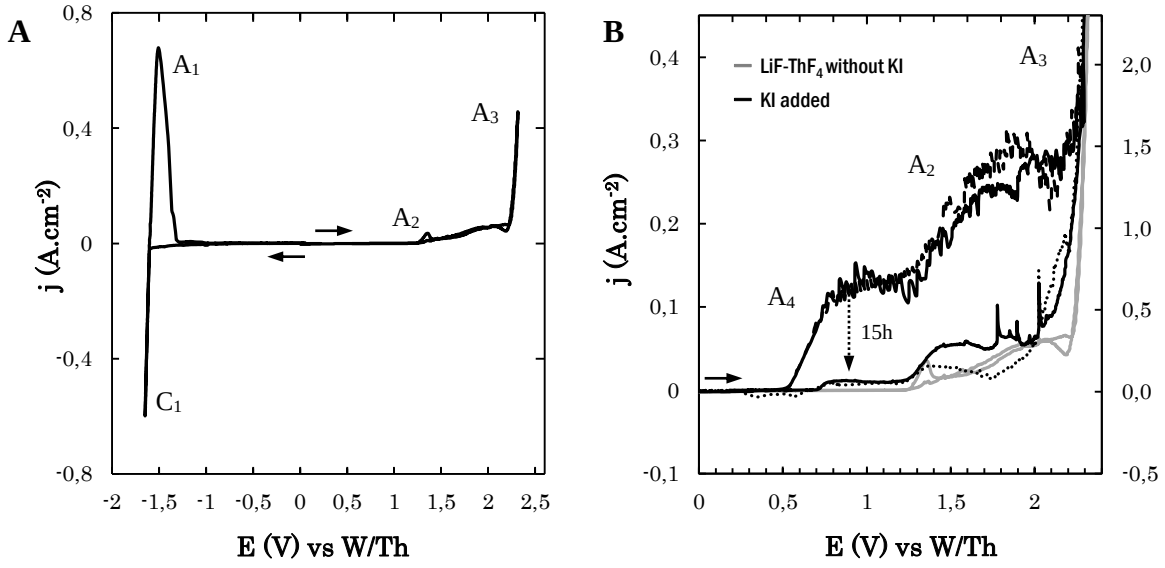

Figure 7. Cyclic voltammograms recorded at 100 mV/s in LiF-ThF_4 (77-23 mol %) at 650°C on a molybdenum electrode (S=0.42 cm^2) and on a gold electrode (S=0.17 cm^2) against NiF_2/Ni reference electrode (A) without and (B) with KI (0.01 mol/kg). Discontinuous line shows the reverse scan. 15 hours after the first addition of KI in LiF-ThF_4 a decrease of the density of current of the CV was recorded on the gold working electrode.

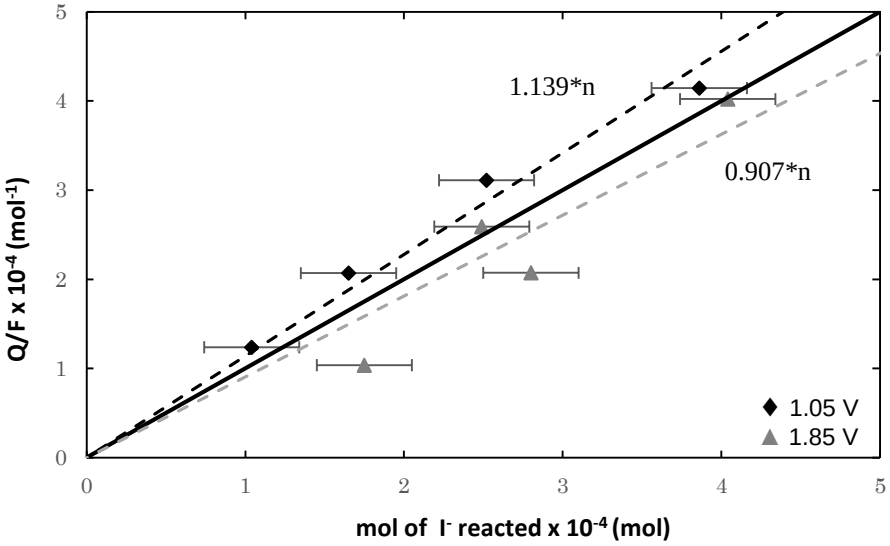

Figure 8. Electric charge consumed during the electrolysis against the quantity of iodide ions oxidized in LiF-ThF_4 at 650°C. Electrolysis realized at +1.05 and +1.85 V *vs* W/Th under argon atmosphere for 30 minutes. Continuous black line represents the theoretical straight line considering 1 exchanged electron.

Table 4. Extraction efficiency of iodide by electrolysis in LiF-ThF_4 at 650°C.

Potential (V) vs W/Th	Efficiency (%)
1.05	95 ± 4
1.85	99 ± 5

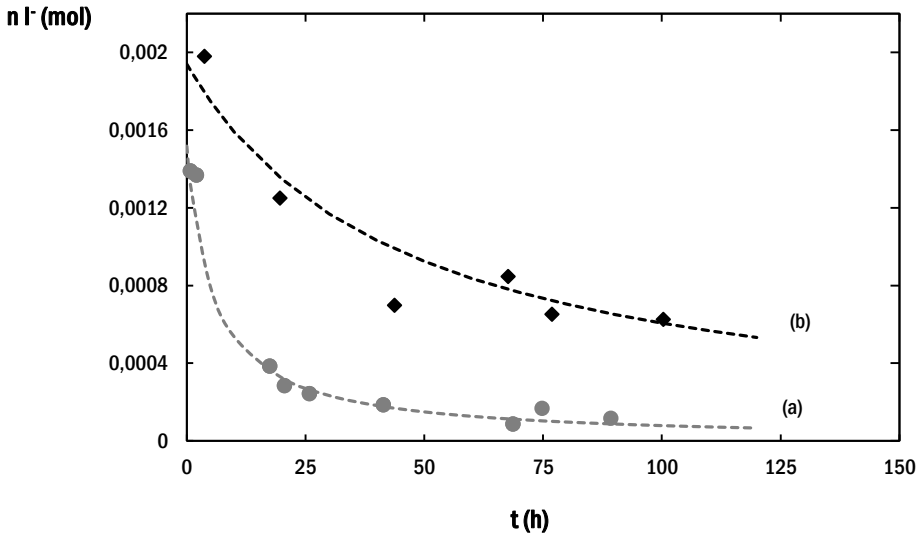

Figure 9. Evolution of the quantity of iodide ions dissolved in LiF-ThF_4 (77-23 mol%) at 650°C under an atmosphere of (a) Argon Alphagaz1: O_2 < 2 ppm and (b) hydrogenated argon (95Ar-5H_2%): O_2 ≤ 5 ppm.

Table 5. Oxidation pseudo kinetic constants of iodide ions and half-life in LiF-ThF_4 at 650°C, under two atmosphere compositions.

Atmosphere	k' ($cm^3/mol^1.s^1$)	$t_{1/2}$ (h)
Argon (O_2 < 2 ppm)	91.1 $.10^{-2}$	5.56
Hydrogenated argon (O_2 ≤ 5 ppm)	6.9 $.10^{-2}$	47.2

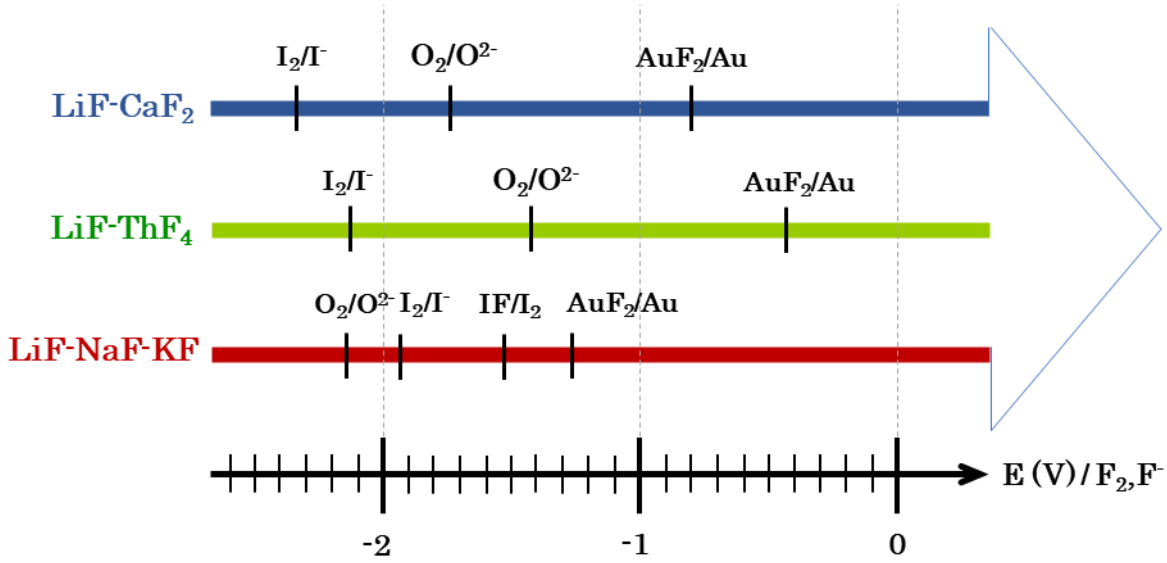

Figure 10. Potential scale representing the redox systems and redox potentials measured through the cyclic voltammograms and referred to the redox potential of F_2/F^- redox couple in the molten LiF-ThF_4 and FLiNaK salts at 650°C.